Opto-Electronic Advances

Supplementary information

2022, Vol. 5, No. 10

DOI: 10.29026/oea.2022.210061

High performance integrated photonic circuit based on inverse design method

Huixin Qi[1], Zhuochen Du[1], Xiaoyong Hu[1,2,3]*, Jiayu Yang[1], SaiSai Chu[1]* and Qihuang Gong[1,2,3]

[1]State Key Laboratory for Mesoscopic Physics & Department of Physics, Collaborative Innovation Center of Quantum Matter & Frontiers Science Center for Nano-optoelectronics, Beijing Academy of Quantum Information Sciences, Peking University, Beijing 100871, China; [2]Peking University Yangtze Delta Institute of Optoelectronics, Nantong 226010, China; [3]Collaborative Innovation Center of Extreme Optics, Shanxi University, Taiyuan 030006, China.

*Correspondence: XY Hu, E-mail: xiaoyonghu@pku.edu.cn; SS Chu, E-mail: chusaisai@pku.edu.cn

This file includes:

Supplementary information for this paper is available at https://doi.org/10.29026/oea.2022.210061

Open Access This article is licensed under a Creative Commons Attribution 4.0 International License.
To view a copy of this license, visit http://creativecommons.org/licenses/by/4.0/.

© The Author(s) 2022. Published by Institute of Optics and Electronics, Chinese Academy of Sciences.

Section 1: High robustness of inverse-design devices

To simplify the calculation, we used the refractive index parameters at wavelength of 1550 nm, the refractive indexes of silicon, air and substrate silica are set as $n_{Si} = 3.46$, $n_{air} = 1$, $n_{SiO_2} = 1.47$, respectively. However, our integrated photonic circuit can work at a broadband of 1500 nm–1600 nm for the high robustness of inverse design method even though the refractive indexes of silicon and silica are different at different wavelengths. We simulate the realization of an all-optical XOR gate when varying the refractive index of the non-air part of the inverse design area. Fig. S1(a) shows the "01", "10" and "11" input states of normalized intensity distribution in the *x*-*y* plane from theoretical calculation when $n = 3.45$. We get "1", "1" and "0" results of corresponding input states, respectively. Figure S1(b–d) show the "01", "10" and "11" input states of normalized intensity distribution in the *x*-*y* plane from theoretical calculation when $n = 3.47$, $n = 3.50$ and $n = 3.60$, respectively. We get "1", "1" and "0" results of corresponding input states, respectively. The transmission of optical signal is sensitive to the refractive index of micro/nano structure, for example, if the refractive index of a resonant ring is changed, the resonant wavelength will change at the same time. Our inverse-design structure has high robustness, so it is not sensitive to the change of the refractive index of inverse design area. Figure S1(a, b) gives the implementation of all-optical XOR gate when $\Delta n = \pm 0.01$. From the normalized intensity distribution in the *x*-*y* plane, we find that the refractive index perturbation will not influence the realization of all-optical XOR gate. Figure S1(c) shows the realization of an all-optical XOR gate with $\Delta n = 0.04$, which can still be realized. Figure S1(d) shows the realization

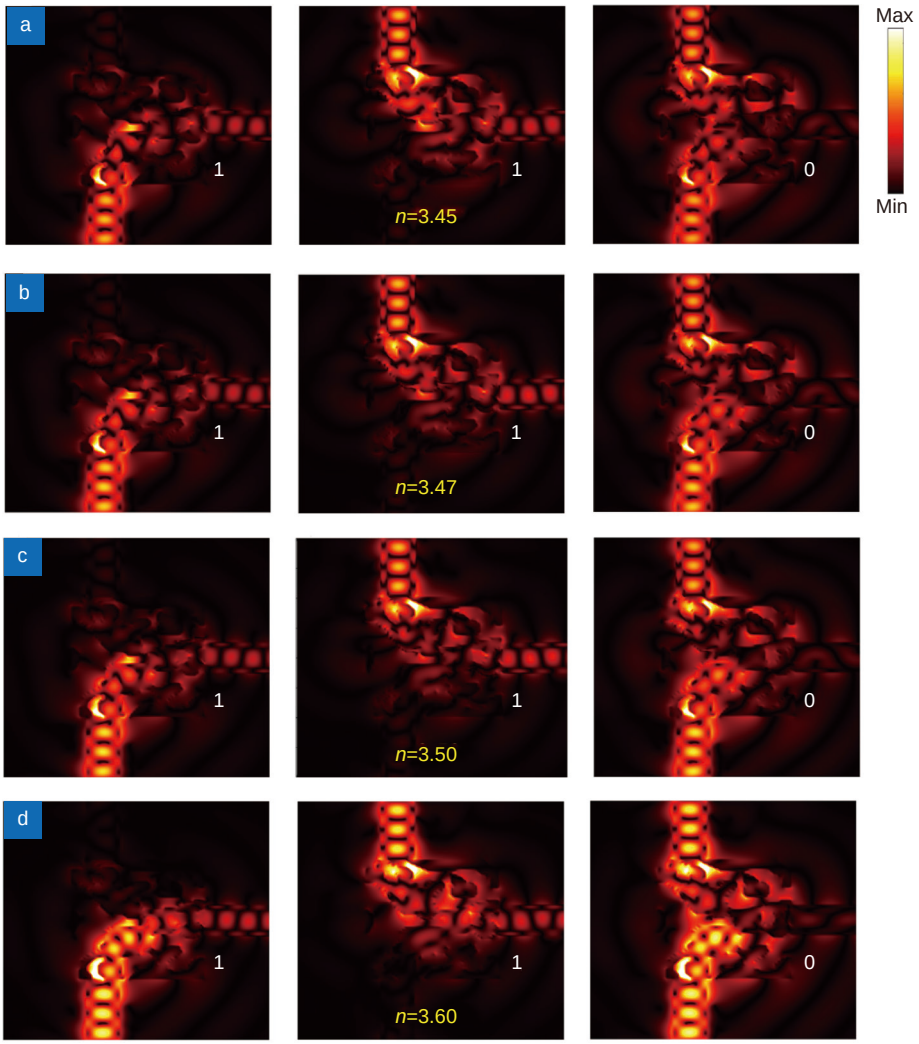

Fig. S1 | Characterization of the all-optical XOR logic gate with different refractive indexes. (**a**) The "01", "10" and "11" states of normalized intensity distribution in the *x*-*y* plane from theoretical calculation when *n*=3.45. (b–d) The "01", "10" and "11" states of normalized intensity distribution in the *x*-*y* plane from theoretical calculation when *n*=3.47, *n*=3.50 and *n*=3.60, respectively.

of all-optical XOR gate with $\Delta n = 0.14$, which can still achieve all-optical XOR gate well.

We also demonstrate the robustness of all-optical switch. Figure S2(a) shows the "ON" state of normalized intensity distribution in the *x*-*y* plane from theoretical calculation when $n = 3.5$. Figure S2(b) shows the "OFF" state of normalized intensity distribution in the *x*-*y* plane from theoretical calculation when $n = 3.5$. Figure S2(c) shows comparation of the transmission simulation results of all-optical switch when $n = 3.46$ and $n = 3.5$. It is found that when the refractive index difference is 0.4, the calculated results still have the property of wideband, which proves that our simplified scheme is reasonable.

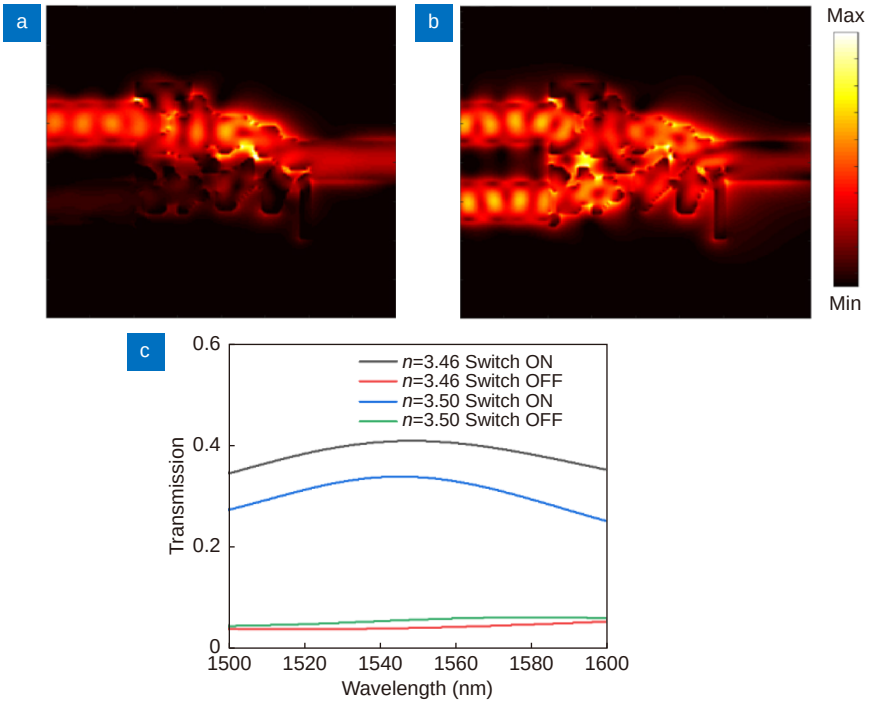

Fig. S2 | Characterization of the all-optical switch with different refractive indexes. (**a**) The "ON" state of normalized intensity distribution in the *x*-*y* plane from theoretical calculation when n_{Si}=3.5. (**b**) The "OFF" state of normalized intensity distribution in the *x*-*y* plane from theoretical calculation when n_{Si}=3.5. (**c**) Comparation of the transmission simulation results of all-optical switch when n_{Si}=3.46 and n_{Si}=3.5.

Section 2: Adjoint method

We start with Maxwell's equations:

$$\nabla \times \boldsymbol{E} = -\frac{\partial \boldsymbol{B}}{\partial t} , \tag{S1}$$

$$\nabla \cdot \boldsymbol{D} = \rho , \tag{S2}$$

$$\nabla \cdot \boldsymbol{B} = 0 , \tag{S3}$$

$$\nabla \times \boldsymbol{H} = \boldsymbol{J} + \frac{\partial \boldsymbol{D}}{\partial t} . \tag{S4}$$

Considering the region of anisotropic, non-ferromagnetic medium without free charge, the equations are written in the frequency domain:

$$\nabla \times \boldsymbol{E} = \mathrm{i}\omega \boldsymbol{B} , \tag{S5}$$

$$\nabla \cdot (\varepsilon \boldsymbol{E}) = 0 , \tag{S6}$$

$$\nabla \cdot \boldsymbol{B} = 0 , \tag{S7}$$

$$\nabla \times \boldsymbol{B} = \mu_0 \boldsymbol{J} - \mathrm{i}\omega\varepsilon\mu_0 \boldsymbol{E} . \tag{S8}$$

Substitute Eq. (S5) into Eq. (S8)

$$\nabla \times \left(-\frac{\mathrm{i}}{\omega}\nabla \times \boldsymbol{E}\right) = \mu_0 \boldsymbol{J} - \mathrm{i}\omega\varepsilon\mu_0 \boldsymbol{E}\,, \tag{S9}$$

$$\nabla \times (\nabla \times \boldsymbol{E}) - \omega^2 \varepsilon\mu_0 \boldsymbol{E} = \mathrm{i}\omega\mu_0 \boldsymbol{J}\,. \tag{S10}$$

In numerical calculation, space is discretized. Assume that the region considered has a total of n units (that is, the region is discretized into n small regions), then Eq. (S10) can be written as:

$$A\boldsymbol{E} = \mathrm{i}\omega\mu_0 J\,, \tag{S11}$$

where A represents the operator $\nabla \times (\nabla\times) - \omega^2\varepsilon\mu_0$ in the discrete space matrix representation ($R^{n\times n}$), $\boldsymbol{E} \in C^{n\times 1}$, the i^{th} element represents A certain rectangular coordinate component of the electric field value of the i^{th} element, $\boldsymbol{J} \in C^{n\times 1}$, the i^{th} element represents A certain rectangular coordinate component of the conduction current density of the i^{th} element, as source of excitation electromagnetic field.

Our target function can always be defined in terms of the (electric) field. An intuitive example is that we want to maximize the density of electromagnetic field energy flow through a certain section, then the objective function can be written as:

$$f = \int_s (\boldsymbol{E} \times \boldsymbol{H}) \cdot \mathrm{d}\boldsymbol{S} = \sum (\boldsymbol{E} \times \boldsymbol{H}) \cdot \Delta \boldsymbol{S}\,. \tag{S12}$$

In electromagnetic waves, $\boldsymbol{H} \propto \boldsymbol{E}$ (only the norm is proportional), then the objective function can be written (ignoring the proportionality coefficient):

$$f = \sum \boldsymbol{E}^2 \Delta S\,. \tag{S13}$$

For such problems, the independent variable of the objective function is the (electric) field, i.e

$$f = f(\boldsymbol{E})\ . \tag{S14}$$

In the optimization problem, our goal is to find the distribution of the dielectric constant of the region to minimize the objective function.

To keep the problem simple, we first set the permittivity of each unit to be continuously varying.

According to the idea of gradient descent algorithm, we only need to let the dielectric constant "drop one step" along the gradient direction to make the objective function smaller:

$$\varepsilon = \varepsilon - \alpha\frac{\partial f}{\partial \varepsilon}\,, \tag{S15}$$

Here $\varepsilon \in R^{n\times 1}$, the i^{th}element represents the dielectric constant of that unit, α is the step length, $\dfrac{\partial f}{\partial \varepsilon} \in R^{n\times 1}$, the i^{th}element represents $\dfrac{\partial f}{\partial \varepsilon_i}$. Notice that the objective function does not explicitly contain ε. So to compute $\dfrac{\partial f}{\partial \varepsilon}$, we need:

$$\frac{\partial f}{\partial \varepsilon} = \frac{\partial E}{\partial \varepsilon}\frac{\partial f}{\partial E}\,, \tag{S16}$$

$\dfrac{\partial E}{\partial \varepsilon} \in C^{n\times n}$, the i^{th} row and j^{th}column represents $\dfrac{\partial E_j}{\partial \varepsilon_i}$, $\dfrac{\partial f}{\partial E} \in C^{n\times 1}$, the i^{th}element represents$\dfrac{\partial f}{\partial E_i}$. Because the dependence of f on the electric field is defined by us, so $\dfrac{\partial f}{\partial E}$ can be figured out by definition. Note that f can depend on the three right-angled components of the electric field. The E in Eq.(S16) represents only one right-angled component, and the rest of the terms are of the same form. The key point of the problem lies in the calculation of $\dfrac{\partial E}{\partial \varepsilon}$. To make the form clear, the matrix and vector are written by the way of index and the Einstein summation convention is adopted:

$$A_{kj}E_j = \mathrm{i}\omega\mu_0 J_k\,. \tag{S17}$$

Take the partial derivative of both sides for ε_i:

$$\frac{\partial A_{kj}}{\partial \varepsilon_i}E_j + A_{kj}\frac{\partial E_j}{\partial \varepsilon_i} = 0$$

$$\frac{\partial E_j}{\partial \varepsilon_i} = \left(A^{-1}\right)_{kj} \frac{\partial A_{kl}}{\partial \varepsilon_i} E_l$$

$$\frac{\partial A_{kl}}{\partial \varepsilon_i} = -\omega^2 \mu_0 \delta_{ik} \delta_{kl} (\text{ We don't sum over } k)$$

$$\frac{\partial E_j}{\partial \varepsilon_i} = -\omega^2 \mu_0 \left(A^{-1}\right)_{ij} E_i \,(\text{We don}'\text{t sum over } i) \ ,$$

$$\frac{\partial f}{\partial \varepsilon_i} = \frac{\partial E_j}{\partial \varepsilon_i} \frac{\partial f}{\partial E_j} = -\omega^2 \mu_0 \left(A^{-1}\right)_{ij} E_i \frac{\partial f}{\partial E_j} \,(\text{We don}'\text{t sum over } i)$$

$$\frac{\partial f}{\partial \varepsilon_i} = -\omega^2 \mu_0 \left(A^{-1} \frac{\partial f}{\partial E}\right)_i E_i \,(\text{We don}'\text{t sum over } i) \,. \tag{S18}$$

Considering that we have figured $\frac{\partial f}{\partial E}$, we can take it as an equivalent source, i.e

$$\mathrm{i}\omega\mu_0 J' = \frac{\partial f}{\partial E} \,. \tag{S19}$$

It is obtained by numerical calculation $E' = A^{-1}\left(\mathrm{i}\omega\mu_0 J'\right)$. The gradient can be expressed as:

$$\frac{\partial f}{\partial \varepsilon_i} = -\omega^2 \mu_0 E_i' E_i \,. \tag{S20}$$

Therefore, we only need to perform two numerical calculations to get the field distribution, and then we can get the gradient of the objective function for the dielectric constant.

Section 3: Optimization of all-optical XOR logic gate based on adjoint method

The lower surface of the all-optical XOR logic gate is a silica substrate layer with a thickness of 2 μm and the background is air. M has a thickness of 220 nm, a horizontal dimension of 2 μm × 2 μm, and the two-dimensional cross-section of M is divided into 50×50 identical units, each of which is a 40 nm × 40 nm square with two choices: etched or unetched, that is, air or Si.

We get the electric field distribution E_1 of the two-dimensional cross-section of inverse-designed area M when the signal light inputs. According to the design requirements of device functions, we set the phase same between signal light Signal1 and signal light Signal2 in the design process for the input direction of two signal lights is different. Other parameters are the same, we get the electric field distribution E_2 of the two-dimensional cross-section of M when the signal light Signal2 inputs. We place an accompanying light at the output waveguide WG3, where the accompanying light is input in WG3. The parameters of the accompanying light are the same as the signal light. We get the electric field distribution E' of the two-dimensional cross-section of M when the accompanying light inputs. Therefore, we calculate the gradient value G_{1i} of the i^{th} iteration, given by:

$$G_{1i} = \frac{\partial f}{\partial \varepsilon_i} = -\omega^2 \mu_0 E' E_1 \,. \tag{S21}$$

The gradient value G_{2i} of the i^{th} iteration, given by:

$$G_{2i} = \frac{\partial f}{\partial \varepsilon_i} = -\omega^2 \mu_0 E' E_2 \ , \tag{S22}$$

where ω is the frequency of the signal light, μ_0 is the vacuum permeability, E' is the two-dimensional cross-section electric field distribution of the accompanying light, E_1 is the two-dimensional cross-section electric field distribution when the signal light inputs, E_2 is the two-dimensional cross-section electric field distribution when the control light inputs. Therefore, we calculate the final gradient of the i^{th} iteration:

$$G = G_{1i} + G_{2i} \ , \tag{S23}$$

Then we get the permittivity distribution of the $(i+1)^{\text{th}}$ iteration:

$$\varepsilon_{i+1} = \varepsilon_i - \alpha G \,. \tag{S24}$$

The whole optimization process can be divided into two steps: continuous optimization process and discrete optimization process. In the continuous optimization process, we set the bias factor to be small, while in the discrete optimization process, we set the bias factor to be large. The refractive index of each basic unit is optimized by using the bias factor β, which is used to control the change speed and magnitude of the refractive index.

Section 4: Experiment realization of all-optical integrated photonic circuit

Controlling the input states of the two beams of light is the one of the most important conditions to realize our all-optical devices. In the process of realizing all-optical switch, the intensity and phase of the signal light and control light should be the same, so we use the same input light in the experiment. As shown in Fig. S3(a), during the whole measurement, a super continuous laser (YSL SC-5) was used to excite the signal light from the single-mode fiber. By carefully adjusting the position and angle of the incident fiber, the signal light is focused on the grating coupler and then coupled into the waveguide. Another single-mode fiber is symmetrically placed at the output coupling end of the grating coupler to collect the output signal light through near-field coupling. We normalized transmission by using reference samples with the same grating coupler parameters but with no nano-structures. After coupling to the waveguide, the signal light is divided into two identical parts through a Y-splitter and then input into the two waveguides of the inverse-design structure, respectively. In this way, the input state is the same as that set in our simulation, and the measurement of the "OFF" state of the all-optical switch can be realized. The insert figure is the scanning electron microscopy (SEM) of inverse-design all-optical switch. In order to ensure the accuracy of the test results, only the upper input waveguide was retained when testing the "ON" state of the all-optical switch, and the signal light was input in the upper waveguide, as shown in Fig. S3(b). Other conditions were consistent with Fig. S3(a). The insert figure is the SEM of tested structure. We also tested the case of the control light input separately, as shown in Fig. S3(c). We retained the waveguide input at the bottom, and the control light input in the bottom waveguide. The insert figure is the SEM of tested structure.

In the process of realizing all-optical XOR logic gate, the intensity and phase of two signal lights should be the same, so we use the same input light in the experiment. As shown in Fig. S3 (d), the signal light is coupled into the waveguide through the grating coupler, then divided into two identical parts through a Y-splitter and input into the two waveguides of the inverse-design structure, respectively. In this way, the input state is the same as that set in our simulation, and the measurement of the "11" state of the all-optical XOR logic gate can be realized. The insert figure is the scanning electron microscopy (SEM) of inverse-design all-optical XOR logic gate. In order to ensure the accuracy of the test

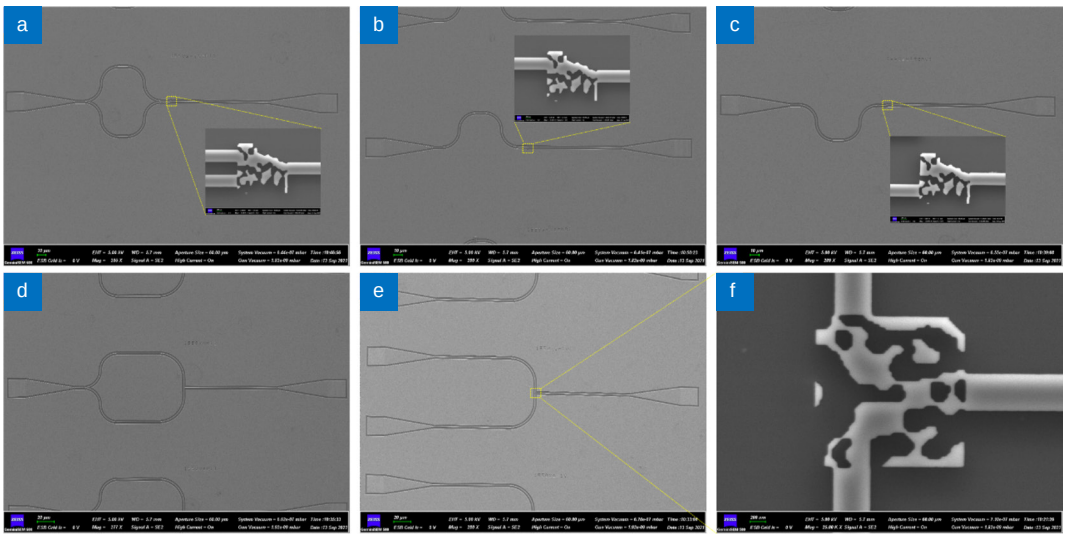

Fig. S3 | Scanning electron microscopy (SEM) image of single inverse-design structure. (**a**) The measurement of the "OFF" state of the all-optical switch. (**b**) The measurement of the "OFF" state of the all-optical switch. (**c**) The measurement of the "11" state of the all-optical XOR logic gate. (**d**) The measurement of the "10" and "01" states of the all-optical XOR logic gate. (**e**) The measurement of the "OFF" state of the all-optical switch. (**f**) Inverse-design structure of the XOR logic gate. The size of the optimized area is 2 μm × 2 μm.

results, the signal light is coupled into the upper waveguide through the upper grating coupler when testing the "10" state of the all-optical XOR logic gate and is coupled into the bottom waveguide through the bottom grating coupler when testing the "01" state, as shown in Fig. S3(e). Figure S3(f) is the SEM of tested structure.

In the following part, we integrated three devices with two all-optical switches controlling the input states of an all-optical XOR logic gate. Similarly, the intensity and phase of four input lights should be the same, so we use the same input light in the experiment. As shown in Fig. S4 (a), the signal light is coupled into the waveguide through the grating coupler, then divided into two identical parts through a Y-splitter and divided into four identical parts through two vertical Y-splitters, next input into the four waveguides of the inverse-design structure, respectively. In this way, the input state is the same as that set in our simulation, and the measurement of the "1111" state of the all-optical integrated circuit can be realized, corresponding to the two all-optical switches are "OFF" states and the XOR gate is "00" state. In this way, the incident mode is the same as that set in our simulation. The input state of "1010" can be tested by keeping only one input waveguide on top and one input waveguide on bottom, as shown in Fig. S4 (b). In other words, two all-optical switches are "ON" states and the XOR gate is "11" state. Fig. S4(c) shows the scanning electron microscopy (SEM) of inverse-design all-optical integrate circuit. As shown in Fig. S4(d), we remove an upper input waveguide to test the input state of "1011", that is, the upper all-optical switch is "ON" state, the lower all-optical switch is "OFF" state, and the all-optical XOR gate is in the input state of "10". Remove an input waveguide below, as shown in Fig. S4(e), to test the input state of "1110", that is, the upper all-optical switch is "OFF" state, the lower all-optical switch is "ON" state, and the all-optical XOR gate is in the input state of "01". Figure S4(f) is a stereogram of inverse-design structure used for measurement.

Section 5: The response time of all-optical integrated circuit

The basic operating principle of all-optical switch is as follows: through the scattering of the inverse-design disordered nanostructures, the mode field distribution of signal light is changed. When the signal light inputs, it can transmit through the disordered nanostructures. When the control light inputs, the mode field of two lights coherently overlays, which changes the mode field distribution of the signal light and the control light, thus the signal light cannot transmit through the disordered nanostructures. To study the time response property of the all-optical switch, we calculated the transmission with a different time delay of the signal light and the control light. Fig. S5(a) shows the normalized intensity distribution of 1550 nm in the *x*-*y* plane from theoretical calculation when the time delay was 0 fs, where the electric field intensity of the output waveguide was low, corresponding to the "OFF" state. Fig. S5(b–g) show the normalized in-

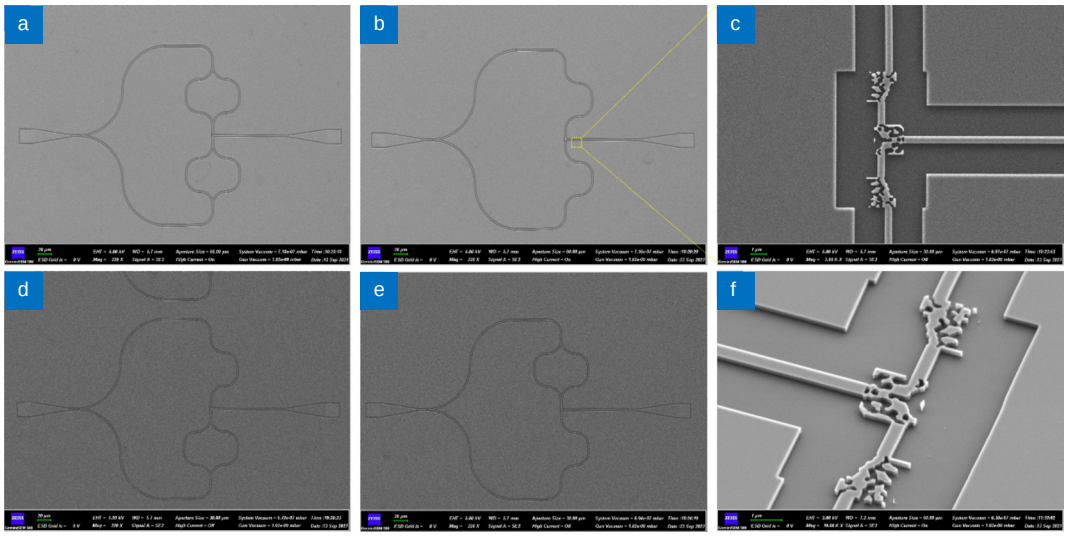

Fig. S4 | Scanning electron microscopy (SEM) image of all-optical integrate circuit. (**a**) The measurement of the "1111" state of the all-optical integrated circuit. (**b**) The measurement of the "1010" state of the all-optical integrated circuit. (**c**) Inverse-design structure of the all-optical integrated circuit. The size of the optimized area is 2.5 μm × 7 μm. (**d**) The measurement of the "1111" state of the all-optical integrated circuit. (**e**) The measurement of the "1010" state of the all-optical integrated circuit. (**f**) The three dimensional figure of inverse-design structure.

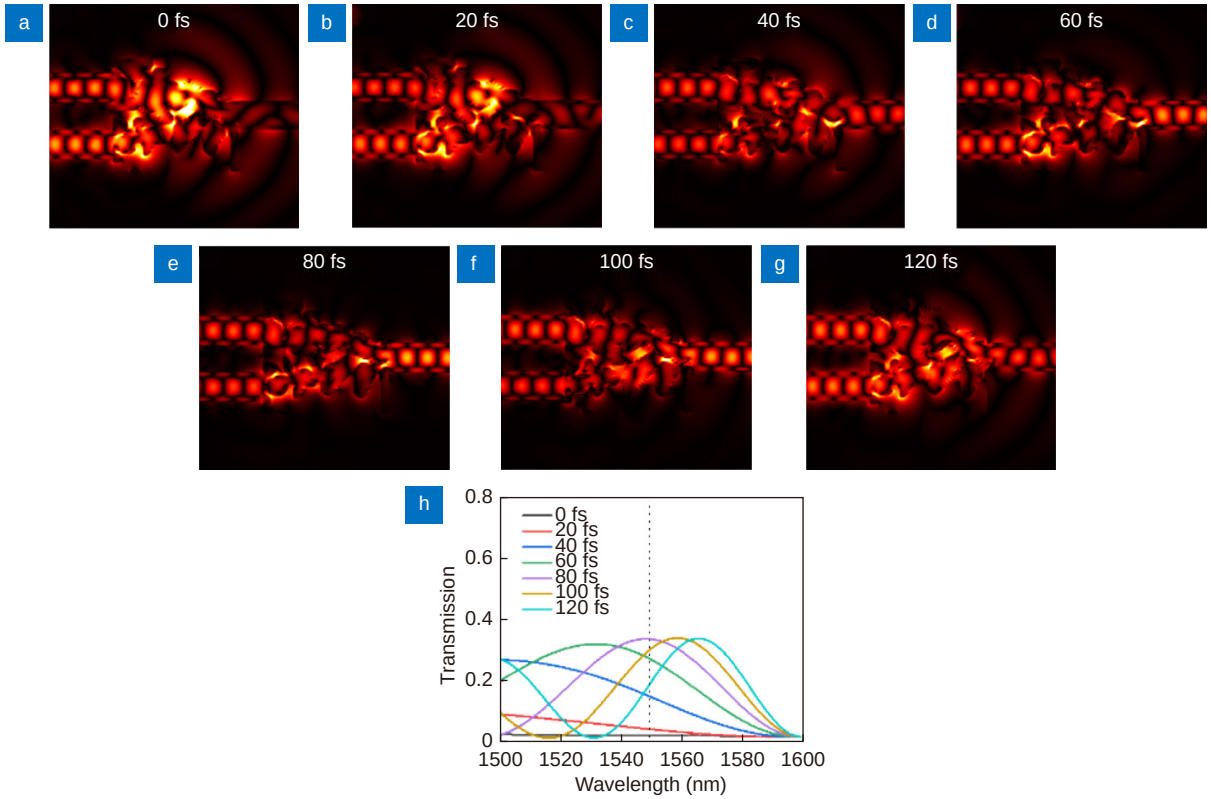

Fig. S5 | Characterization of the all-optical switch. (**a**) The "OFF" state of normalized intensity distribution in the *x*-*y* plane from theoretical calculation at *t*=0 fs. (**b**–**g**) The "ON" state of normalized intensity distribution in the *x*-*y* plane from theoretical calculation at *t*=20 fs, 40 fs, 60 fs, 80 fs, 100 fs and 120 fs, respectively. (**h**) Transmission of the output of the all-optical switch under different delay time at 1500 nm-1600 nm. Insert is transmission of the output of the all-optical switch under different delay time at 1500 nm.

tensity distribution of 1550 nm in the *x*-*y* plane from theoretical calculation when the time delay was 20 fs, 40 fs, 60 fs, 80 fs, 100 fs and 120 fs, respectively. According to the simulated results, when the time delay is 80 fs, the switch can achieve a maximum switching contrast of 13 dB. Figure S5(g) shows transmission of the output of the all-optical switch under different delay time at 1500 nm–1600 nm. For all-optical XOR logic gate, we only need to control the phase and intensity of the two signal lights identical, so we defined the propagation time of the light in the structure as the response time of the XOR logic gate. The footprint of a single device is 2 μm × 2 μm, so for the all-optical XOR logic gate, the propagation time of the signal light is the response time of the optical XOR logic gate based on the linear light principle. The theoretical response time is 23 fs. We integrated three devices with two all-optical switches controlling the input states of an all-optical XOR logic gate. Here, the response time is the addition of the switch and the XOR logic gate, which is less than 150 fs.

Section 6: Function of identifying two-digit logic signal results

Our integrated photonic circuit also realizes the function of identifying whether two two-digit numbers are equal or not. When logic signal 1 is equal to logic signal 2, the identifying result of the circuit is 0. When logic signal 1 is different from logic signal 2, the identifying result of the circuit is 1. Such function plays an important part in logic information processing.

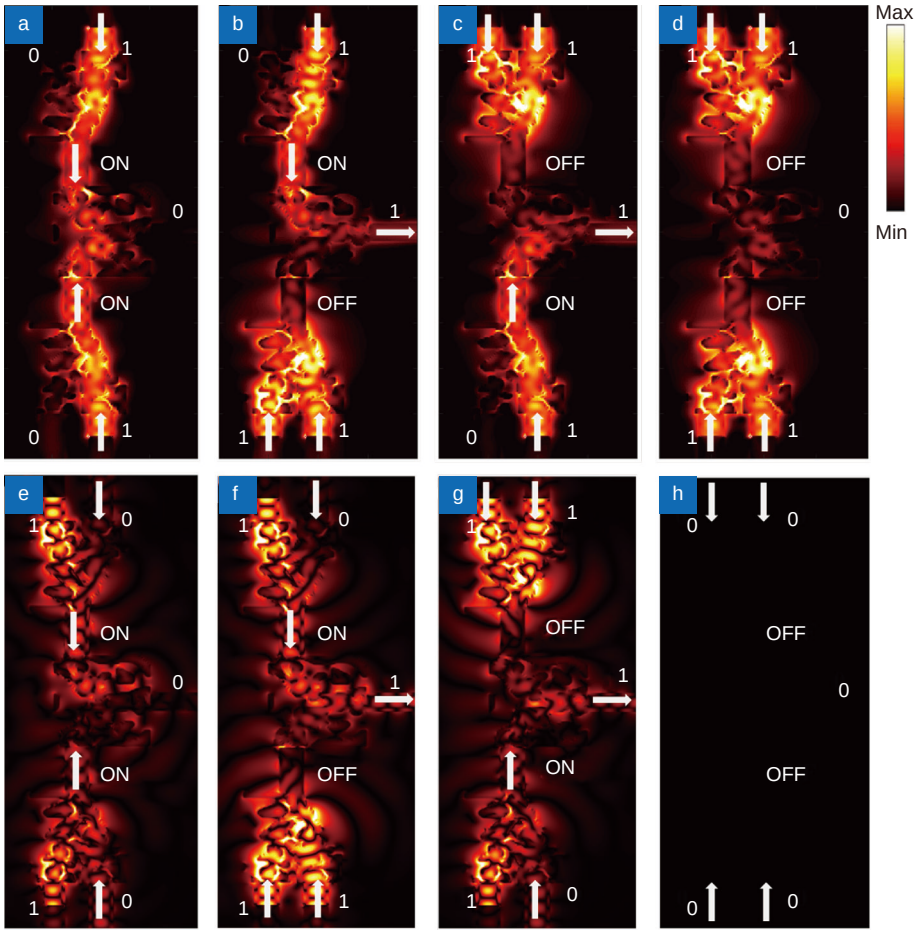

Fig. S6 | Function of identifying two-digit logic signal results. (**a**) The results of identifying “10” and “10”. (**b**) The results of identifying “10” and “11”. (**c**) The results of identifying “11” and “10”. (**d**) The results of identifying “11” and “11”. (**e**) The results of identifying “01” and “01”. (**f**) The results of identifying “01” and “11”. (**g**) The results of identifying “11” and “01”. (**h**) The results of identifying “00” and “00”.